This version of the supplementary information was updated on 2nd March 2021 to correct errors in Figure S12, Table S1, and minor errors in the text.

Supporting Information for:

Nitrate Removal from Reverse Osmosis Concentrate in Pilot-Scale Open-Water Unit Process Wetlands

Rachel C. Scholes[a,c], Michael A. Vega[b,c], Jonathan O. Sharp[b,c], David L. Sedlak[a,c]

[a]Department of Civil and Environmental Engineering
University of California
Berkeley, California 94720
United States

[b]Department of Civil and Environmental Engineering
Colorado School of Mines
Golden, Colorado 80401
United States

[c]NSF Engineering Research Center for Reinventing the Nation's Urban Water Infrastructure (ReNUWIt)

Number of pages: 23 Figures: 12 Tables: 3

Table of Contents

1 Materials & Methods

1.1 Pilot treatment system diagram

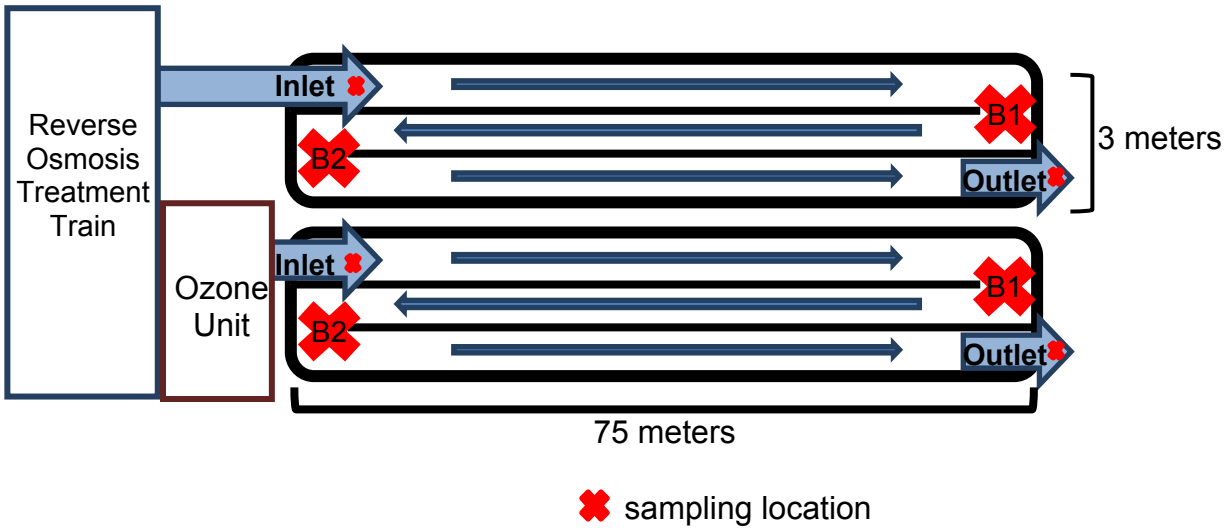

Figure S1. Pilot treatment system. Cell 1 (top) received RO concentrate without pre-treatment, whereas Cell 2 received ozonated RO concentrate. B1 = Baffle 1, B2 = Baffle 2.

1.2 Tracer tests

Method

Tracer tests were conducted in both pilot-scale treatment cells using lithium bromide as a conservative tracer. For each cell, 500 g of LiBr was dissolved in a 5-gallon bucket with RO concentrate. The dissolved LiBr was then added to the wetland cell inflow by slowly pouring the solution into the cell inlet. The effluent of the cell was sampled using a 24-sample autosampler (~100 mL/sample) at 3-6 hour intervals for 8-9 days following the introduction of tracer. All samples were transported to the laboratory and bromide was analyzed using ion chromatography.

Results

Background bromide concentrations (measured in effluent samples collected prior to tracer introduction) were subtracted from effluent bromide concentrations. Background-subtracted results are shown in Figure S2. Mean hydraulic residence times were calculated using the tanks-in-series model (Cell 1 HRT = 3.6 days, Cell 2 HRT = 2.9 days). Effluent samples were also analyzed for lithium to confirm HRT calculations (data not shown) and resulted in similar values (Cell 1 HRT = 3.5 days, Cell 2 HRT = 3.0 days).

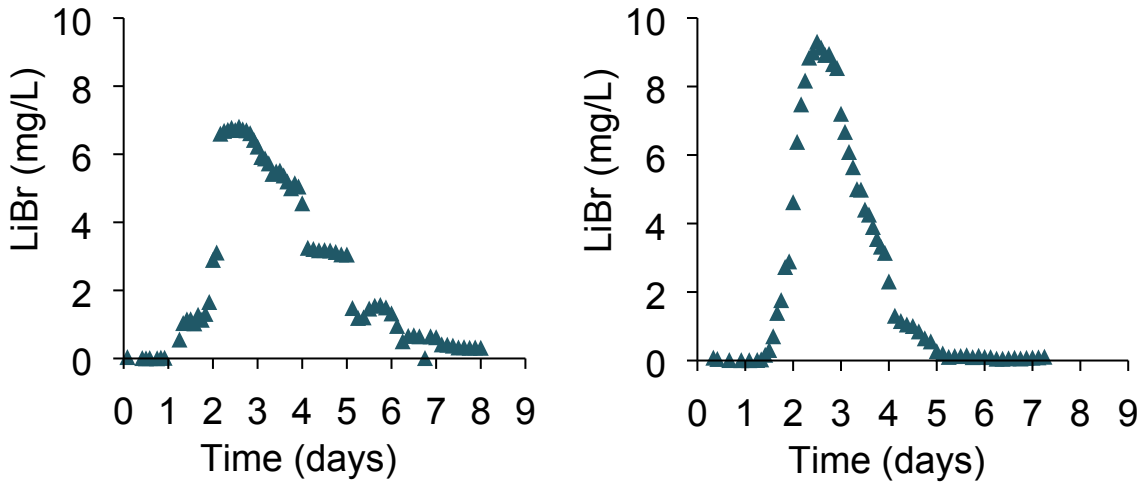

Figure S2. Background-subtracted effluent bromide concentrations during tracer tests for Cell 1 (left) and Cell 2.

1.3 Biomat sequencing and qPCR methods

Amplification of *nir*K and *nar*G genes by quantitative PCR (qPCR) was performed using a QuantStudio3 Real-Time PCR System using Power SYBR™ Green MasterMix (Applied Biosystems, Foster City, CA, USA) in 25 µL reactions containing ~1 ng (2 µL) template DNA. For normalization purposes, copies of the 16S rRNA gene were determined using the Zymo Femto™ Bacterial Quantification kit (Zymo Research, Irvine, CA, USA) according to the manufacturer's instructions. Standards for all genes were derived from biomat qPCR amplicons excised from an agarose gel followed by purification using a Zymoclean Gel DNA Recovery Kit, quantification in technical triplicates using a Qubit™ 2.0 Fluorometer (dsDNA HS Kit), then a minimum of six 1:10 dilutions resulting in at least seven total standards of each gene. Standards were amplified in technical triplicate in parallel with non-template and negative extraction controls, and samples were amplified in both technical and biological triplicate (n=9). Thermal profiles and primer sequences for qPCR amplification are reported in Table S1 and amplification specificity and purity was verified by a melt curve step at the end of each qPCR reaction (60° C to 95° C with continuous fluorescence acquisition) to visualize denaturation curves specific to each product, as well as with a single band of the expected size on a 2.5% agarose gel stained with GelGreen when making standards. Threshold cycles were calculated using QuantStudio 3 Design and Analysis Software (v1.5.1) and reaction efficiencies and linear dynamic ranges are reported in Table S1. Negative controls always amplified a minimum of 3 cycles later than samples, with the exception of 1 out of 9 *nar*G replicates from June 2018 (1 cycle greater than negative controls, 3 cycles greater than the average of the 8 others within the replicate set). All biomat samples collected from Cell 1 in summer 2018 and 2019 months were analyzed (2018: June, July, August; 2019: June, August).

Amplification of DNA for 16S and 18S rRNA gene sequencing was performed with primers that broadly represent all three domains of life, although only 16S rRNA gene amplicons were analyzed for this study. The forward primer 515F-Y (5′-**GTA AAA CGA CGG CCA G** CCG TGY CAG CMG CCG CGG TAA-3′) contains the M13 forward primer (bold) which is fused to the 515F-Y forward primer (underlined), whereas the reverse primer 926R (5′-CCGYCAATTYMTTTRAGTTT-3′) was unmodified from Parada *et al.*[1], as described by Stamps *et al.*[2] and Kraus *et al.*[3] PCR reactions were performed with 5Prime HotMasterMix using 2 µL DNA template and a final volume of 25 µL. Thermal cycling profiles are presented in Table S1. Products were purified using AmpureXP paramagnetic beads at a final concentration of 0.8X. Purified amplicons were used in a PCR barcoding reaction, purified, and quantified using a Qubit 2.0 Fluorometer. Purified, barcoded, and quantified amplicons were normalized and concentrated with Amicon Ultra-0.5mL 30K Centrifugal Filter Devices. Final pooled and purified concentrates were shipped to the Duke Center for Genomic and Computational Biology (GCB) and sequenced on an Illumina MiSeq platform using a v2 paired-end 2 x 250 bp reagent kit.

Raw reads were demultiplexed with sabre (https://github.com/najoshi/sabre) and imported into R for quality visualization and processing using DADA2.[4] Adapters were manually

trimmed, forward and reverse reads were truncated to 222 and 234 basepairs, and the respective maximum expected errors were limited to 2 and 4 within DADA2's filterandtrim() command. Filtered and trimmed reads were then dereplicated, denoised and merged. Due to the long term nature of the project, samples were sequenced across three distinct runs. A minimum of three samples were re-analyzed on each sequencing run and compared to ensure run effects did not impact time series data; differences were never significant. Error estimations, denoising, dereplicating and merging of forward and reverse reads were performed on samples from unique runs, then the corresponding ASV tables were merged to one prior to removing chimeric sequences, which were removed based on identification by consensus. Taxonomy was assigned using the SILVA v132 database[5] with default DADA2 parameters, excluding the minimum bootstrap confidence level, which was increased from 50 to 80. Unique, non-chimeric sequences were imported into QIIME v1.9.1[6] and aligned with pyNAST[7] against the SILVA v132 database[5]. FastTree[8] was then used to generate a phylogenetic tree. A final ASV table contained 2,145,495 paired-end sequences across 89 samples ranging in depth from 7,397 to 42,252 sequences, including replicate archived samples that were re-sequenced across discrete sequencing runs (n=9); rarefaction was therefore performed to 7,397 sequences. All phylogenetic analyses were performed with and without rarefaction, and chloroplast, mitochondrial and eukaryotic ASVs were excluded to focus on bacterial and archaeal communities. A UniFrac distance matrix[9] was constructed in Phyloseq[10] and used for principal coordinate analysis (PCoA). Detrended correspondence analysis (DCA) was used in parallel where temporal trends demonstrated a significant horseshoe effect.[11] The adonis() test within vegan[12] was used to assess statistical differences in weighted and unweighted UniFrac distance matrices, testing for homogeneous dispersion with each analysis. To quantitatively evaluate differences in microbial community composition between summer 2018 and summer 2019 samples, differential abundance analysis was performed on non-rarefied ASV tables using DESeq2[13]. Heatmaps and ordinations were made using ampvis2[14] and Phyloseq,[10] respectively. Demultiplexed sequences, including control samples that were re-sequenced across discrete sequencing runs throughout the time series, are available in the National Center for Biotechnology Information Short Read Archive (NCBI SRA) under project number PRJNA637567.

Table S1. Primer details, thermal profiles, reaction efficiencies, and linear dynamic ranges for *nar*G,[15] *nir*K,[16,17] and 16S[18] (Zymo Research, personal communcation) for qPCR, as well as 16S/18S PCR for amplicon sequencing.[1]

Target Gene	Primer Name	Primer Sequence (5' - 3')	Primer Concentration [nM]	Amplicon Size [bp]	Thermal Profile	Reaction Efficiency [%]	Linear Dynamic Range [copies]
*nar*G	*nar*G 1960 m2f	TA(CT) GT(GC)GG GCAGA(A G)AAACT G	500	110	95°C 10 min, 6 touchdown cycles (95°C 15 s, 63-58°C (1°C per cycle) 30 s, 72°C 30 s), then 35 cycles (95°C 15 s, 58°C 30 s, 72°C 30 s, 81°C 15 s for fluorescence acquisition)	81.0	1.2×10^1 to 1.2×10^7
	*nar*G 2050 m2r	CGTAGA AGAAGC TGGTGC TGTT	500				
*nir*K	*nir*K 876	ATYGGCG GVAYGGC GA	500	164	95°C 10 min, 6 touchdown cycles (95°C 15 s, 63-58°C (1°C per cycle) 30 s, 72°C 30 s), then 35 cycles (95°C 15 s, 58°C 30 s, 72°C 30 s, 81°C 15 s for fluorescence acquisition)	88.6	6.3×10^1 to 6.3×10^7
	*nir*K 1040	GCCTCGA TCAGRTT RTGGTT	500				
16S	8F	AGAGTTT GATCCTG GCTCAG	18000	352	95°C 10 min, 36 cycles (95°C 30 s, 50°C 30 s, 72°C 60 s), 72°C 7 min	91.7	4.0×10^4 to 4.0×10^{10}
	357R	GACGACG GAGGGCA TCCTC	18000				
16S / 18S	515F-Y	GTGYCAG CMGCCGC GGTAA	200	~400 (16S); ~600 (18S)	94°C 2 min, then 30 cycles (94°C 45 s, 50°C 45 s, 68°C 90 s), 68°C 5 min	n/a	n/a
	926R	CCGYCAA TTYMTTT RAGTTT	200				

2 Results

2.1 Photosynthetic activity in irradiated carbon amendment microcosms

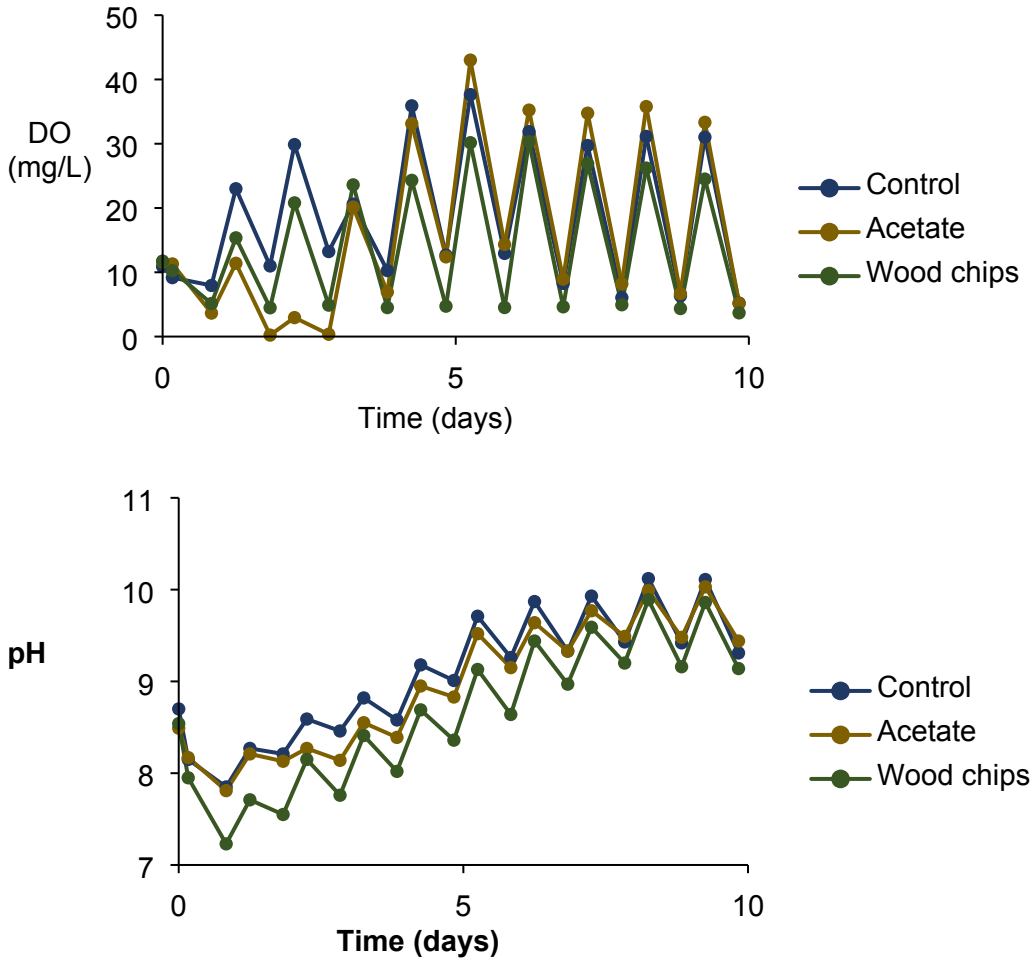

Figure S3. DO and pH measurements taken at the beginning and end of each photoperiod in microcosm experiments without (control) and with carbon amendments.

2.2 Carbon leaching experiments

Experiments were conducted in 200-mL beakers containing 150 mL of DI water or RO concentrate at room temperature and were stirred from above by suspended stir bars. Amendments were placed in polypropylene mesh bags and placed on the bottom of the beaker prior to adding biomat.

Conditions tested:

- 1.5 g woodchips in 150 mL DI water + 5 mM nitrate
- 1.5 g woodchips + 17 g biomat in DI water
- 1.5 g gravel + 17 g biomat in DI water
- 1.5 g woodchips + 17 g biomat in RO concentrate

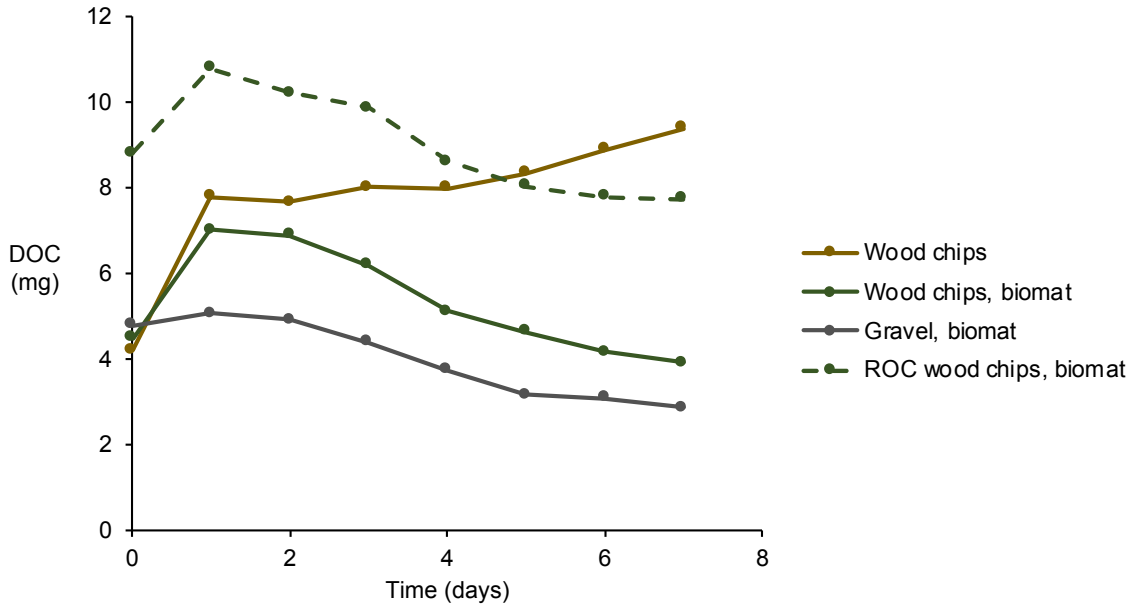

Figure S4. DOC in carbon leaching experiments.

2.3 Area requirement calculations

To compare area requirements across RO recovery rates, we first calculated the photon flux of photosynthetically active radiation (wavelengths between 400-700 nm) incident on the biomat surface, designated *PAR*. For further calculations, *PAR* was held constant at a value equivalent to 70% penetration of PAR through the water column in the pilot-scale open-water wetland, which matches the average PAR penetration observed in the pilot-scale system. The calculated depth of the wetland was thereby adjusted to yield the same photon flux for each scenario.

PAR (Ein/m^2-s) was calculated as:

$$PAR = \sum_{\lambda = 400-700} Z(\lambda) * S(\lambda)$$

where Z is the daily average sunlight irradiance from SMARTS and S is a light screening factor[19] calculated using absorption spectra ($\alpha(\lambda)$) from inlet RO concentrate at the pilot-scale open-water wetlands:

$$S(\lambda) = \frac{1 - 10^{-1.2\alpha(\lambda)z}}{(2.3)(1.2)\alpha(\lambda)z}$$

Depth, z, was calculated for each RO recovery rate using Solver in Excel (Figure S5). Absorbance ($\alpha(\lambda)$) was adjusted for different RO recovery rates according to Beer's Law.

The area required for 90% nitrate removal at an HRT of 3 days was calculated for each flow rate of RO concentrate ($Q_{concentrate}$) as:

$$A_{90} = \frac{HRT * Q_{concentrate}}{z}$$

The mass of carbon required to fuel denitrification was treated as constant because the same mass of nitrate would be present in the concentrate stream regardless of the concentrate volume. Thus, area requirements become a function only of flow rate and depth.

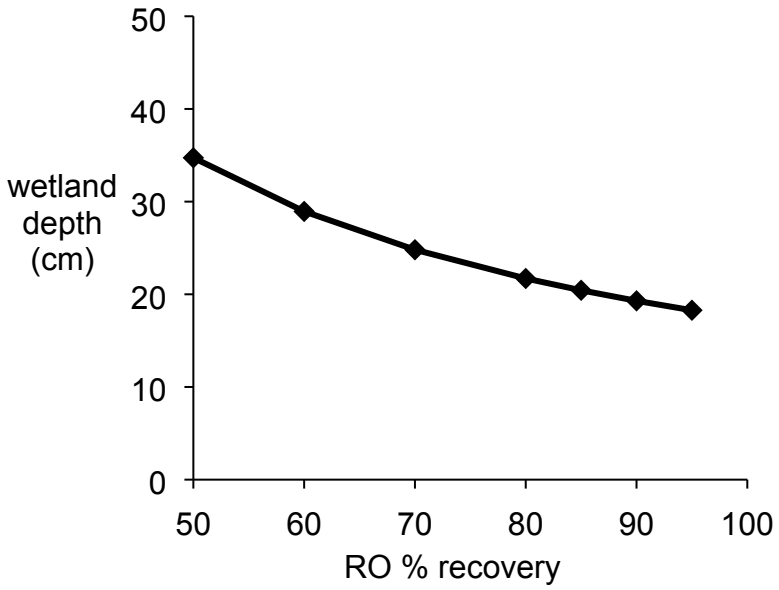

Figure S5. Depth for 70% PAR penetration as a function of recovery of RO treatment.

2.4 Light absorption in RO concentrate

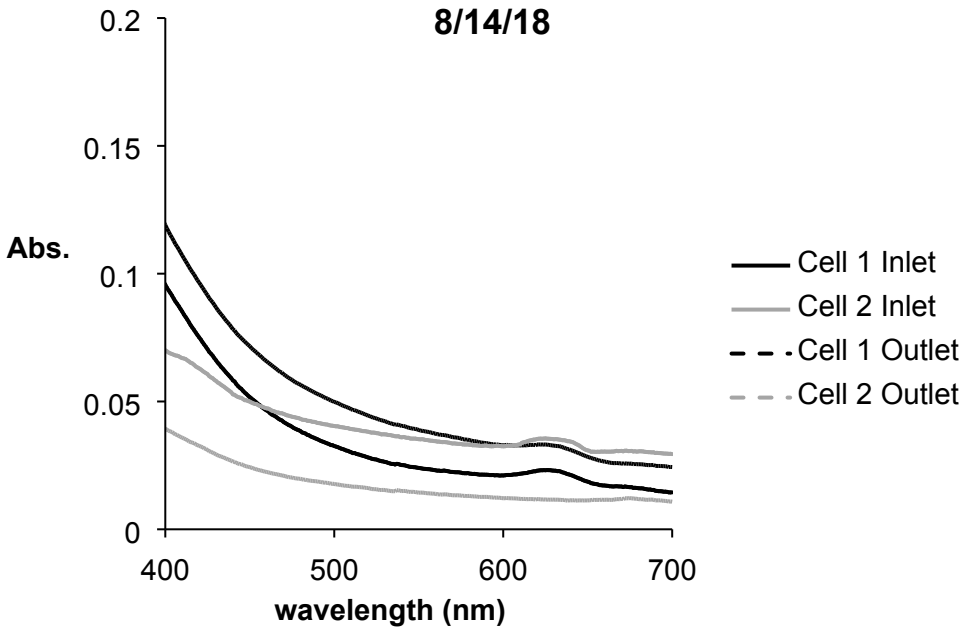

Figure S6. Representative absorbance spectra of unfiltered inlet and outlet samples with and without ozone treatment (path length=1 cm).

2.5 Dissolved organic nitrogen concentrations

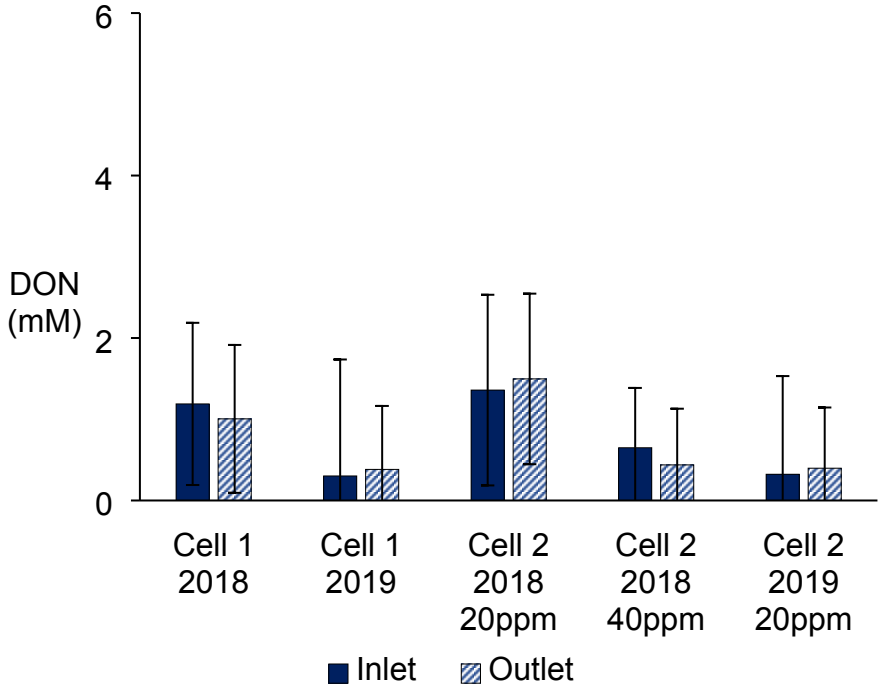

Figure S7. Dissolved organic nitrogen concentrations at the inlet and outlet of the pilot-scale open-water cells. Values represent the average over 6 sampling rounds in the summer of 2018, and 3 sampling rounds in the summer of 2019. Error bars represent the standard deviation.

2.6 Biomat growth and photosynthesis

Table S2. Depth of biomat solids. Biomat depth was similar in both cells at locations >1m from the inlet.

Date	**Biomat Depth Cell 1 Inlet (cm)**	**Biomat Depth Cell 2 Inlet (cm)**	**Avg. Biomat Depth both cells (cm)**
July 2017	0	0	0
April 2018	1.0	4.0	<1.0
July 2018	7.5	10.0	2.5
June 2019	20.0	20.0-22.0	10.0-12.0

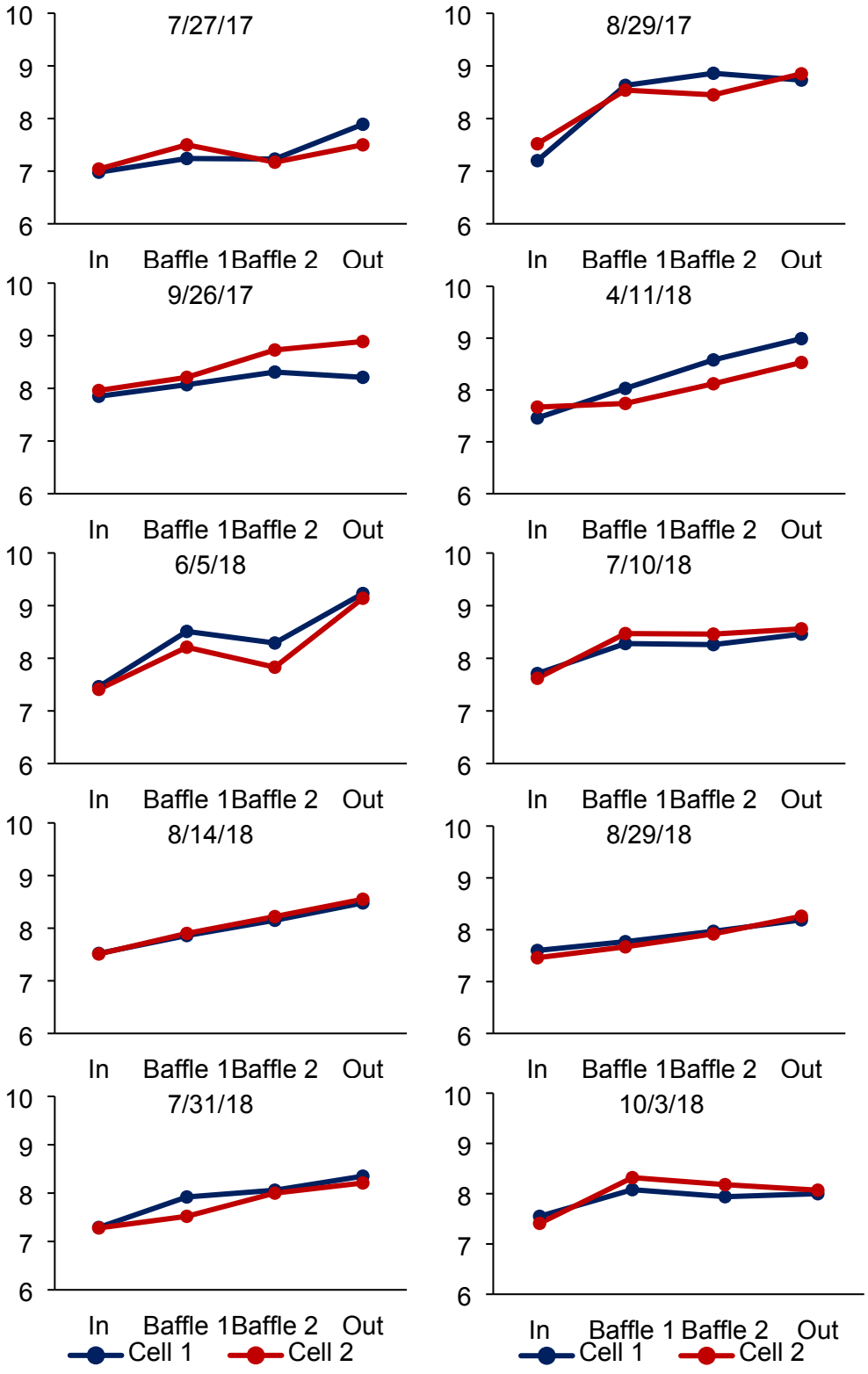

Fig. S8. pH profiles in both cells on sampling dates.

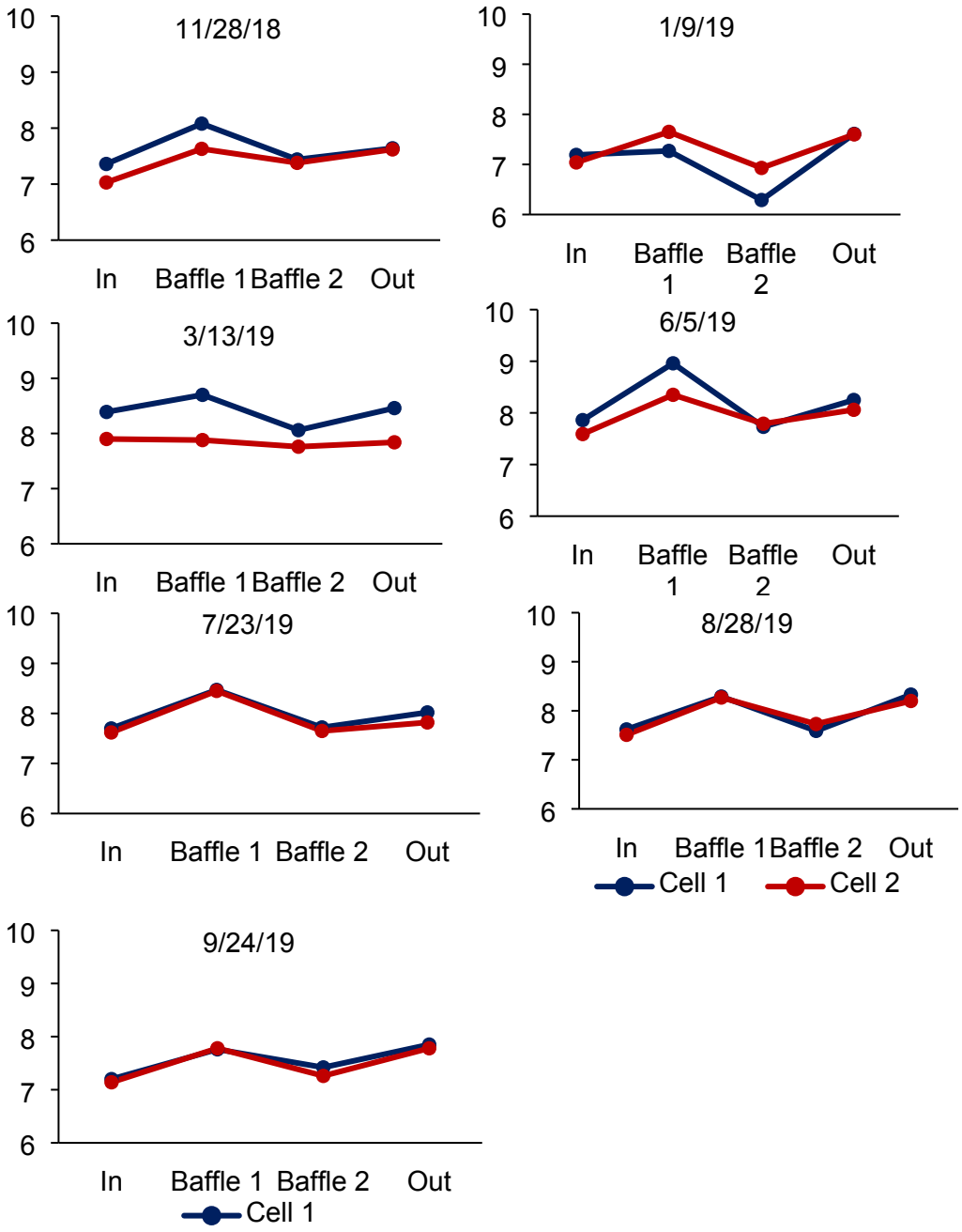

Fig. S8 cont'd. pH profiles in both cells on sampling dates.

2.7 Biomat ecological assessment

Multiple ordination methods (ie., PCoA, DCA) were used to visualize differences in biomat communities that received ozonated influent versus those that did not. To test the hypothesis that ozone pre-treatment caused a shift in microbial community structure, a Permutational Multivariate Analysis of Variance (PERMANOVA) was run using adonis() within the R package Vegan[12] and employing weighted and unweighted UniFrac distance matrices.[9] A beta dispersion test was also run to confirm or reject the hypothesis that dispersion was homogeneous within the tested sample groupings. Biomat microbial communities were not significantly different ($p > 0.05$) between cells at any sampling event (Figure S9a,b; Table S3). Further, we failed to reject the null hypothesis for the beta dispersion test, confirming that sample groupings had equivalent dispersions (Table S3). However, DCA ordinations suggested that the communities might be divergent during the second year of operation (Figure S9c). Importantly, UniFrac distance matrices incorporate phylogenetic relationships by weighting community structure by the fraction of branch lengths on a community tree that are unique, and DCA ordinations utilize ASV tables, rather than distance matrices, missing useful phylogenetic information. Though it is possible that ozonation may have selected for certain taxa, we conclude that the bacterial and archaeal communities were not significantly different between cells based on adonis tests of UniFrac distance matrices and similarities in functional chemical monitoring data (Figure 2, S7, S8). Lastly, phylogenetic comparisons of the pilot-scale cells were qualitatively complemented by inspection of diatom communities using SEM and light microscopy; no significant differences were observed throughout the 2-year monitoring period.

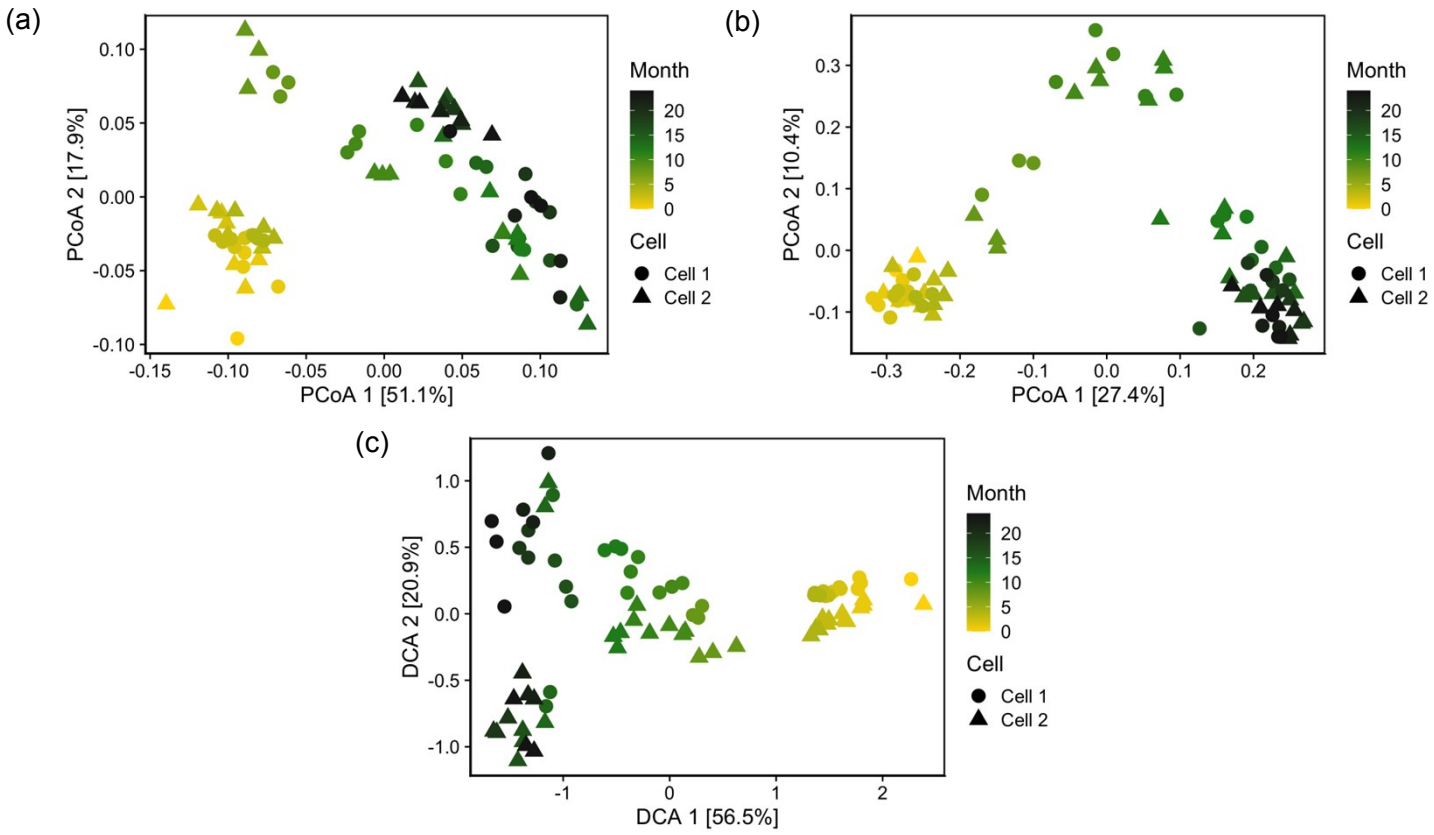

Figure S9. Ordination plots depicting changes in the structure of 16S rRNA gene microbial communities over time and between cells. **(a-b)** PCoA ordinations of weighted and unweighted UniFrac distance matrices suggest that microbial communities were not significantly different between cells at any timepoint (Table S3). **(c)** A DCA ordination decreased the horseshoe effect associated with RO concentrate biomat community temporal evolution by dividing points into segments along DCA1, then re-scaling these segments along DCA2, minimizing arching and clearly demonstrating the influence of time along DCA1. However, DCA2 suggests divergence of communities as a function of cell during the second year of operation. See Section 2.7 and Table S3 for further analysis. All ordinations were performed on both rarefied and non-rarefied ASV tables, but only rarefied are shown.

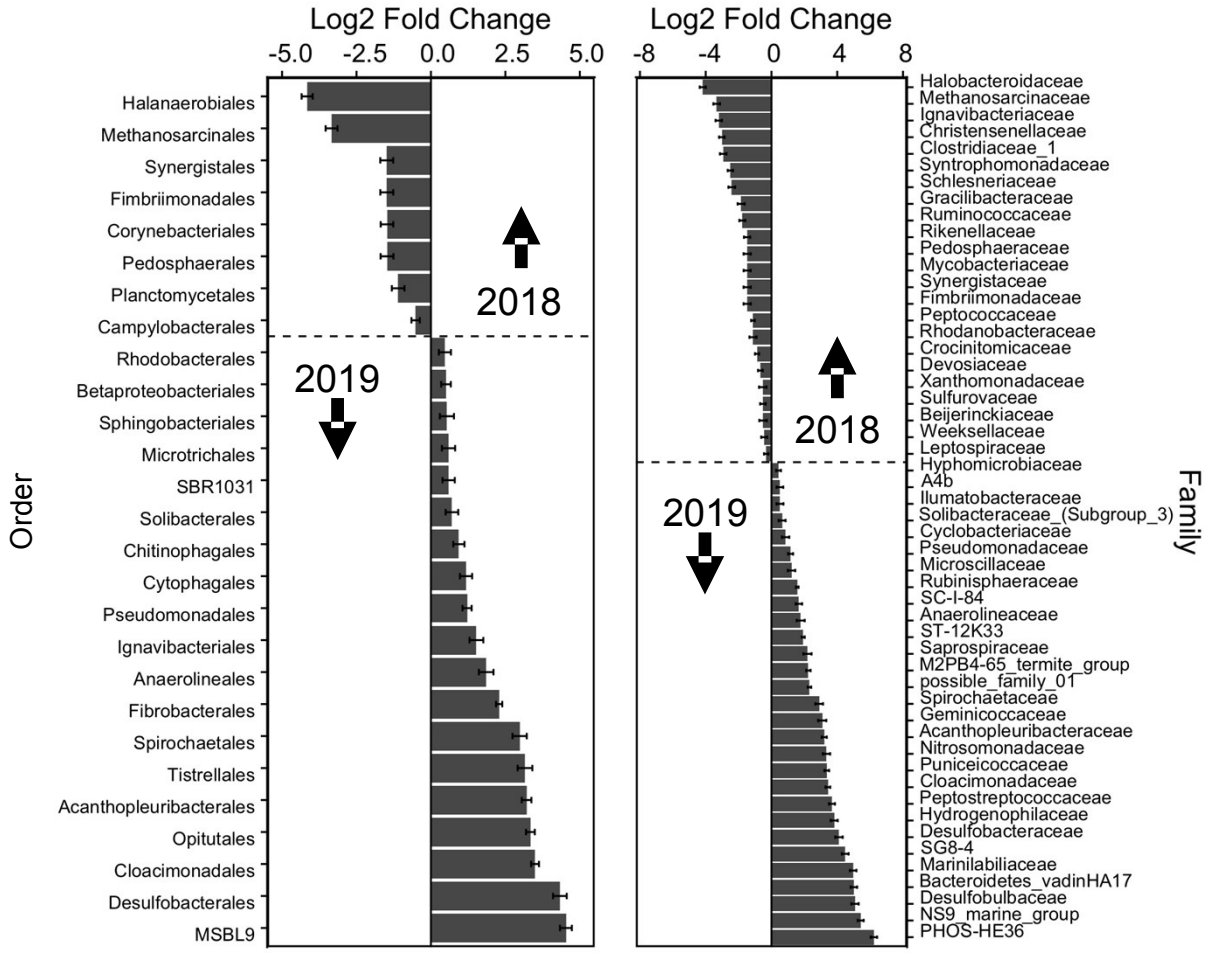

Figure S10. Differential abundance analysis (performed using DESeq2[13]) visualized as $Log_2FoldChange$ between summer 2018 and 2019 RO concentrate biomat microbial communities generally revealed increases in clades known to contain species capable of denitrification (e.g., Betaproteobacterales, *Hydrogenophilaceae*, *Nitrosomonadaceae*, *Pseudomonadaceae*, etc.),[20–22] sulfate reduction (e.g., Desulfobacterales, *Desulfobacteraceae*, *Desulfobulbaceae*, etc.),[23,24] and complex carbon degradation (e.g., *Saprospiraceae*, Fibrobacterales, etc.),[25,26] consistent with increased thickness and visual observations of biomat maturity. Taxa below the dashed line were significantly more abundant in 2019 communities relative to 2018. Both cells were collectively considered due to a lack of statistical differences.

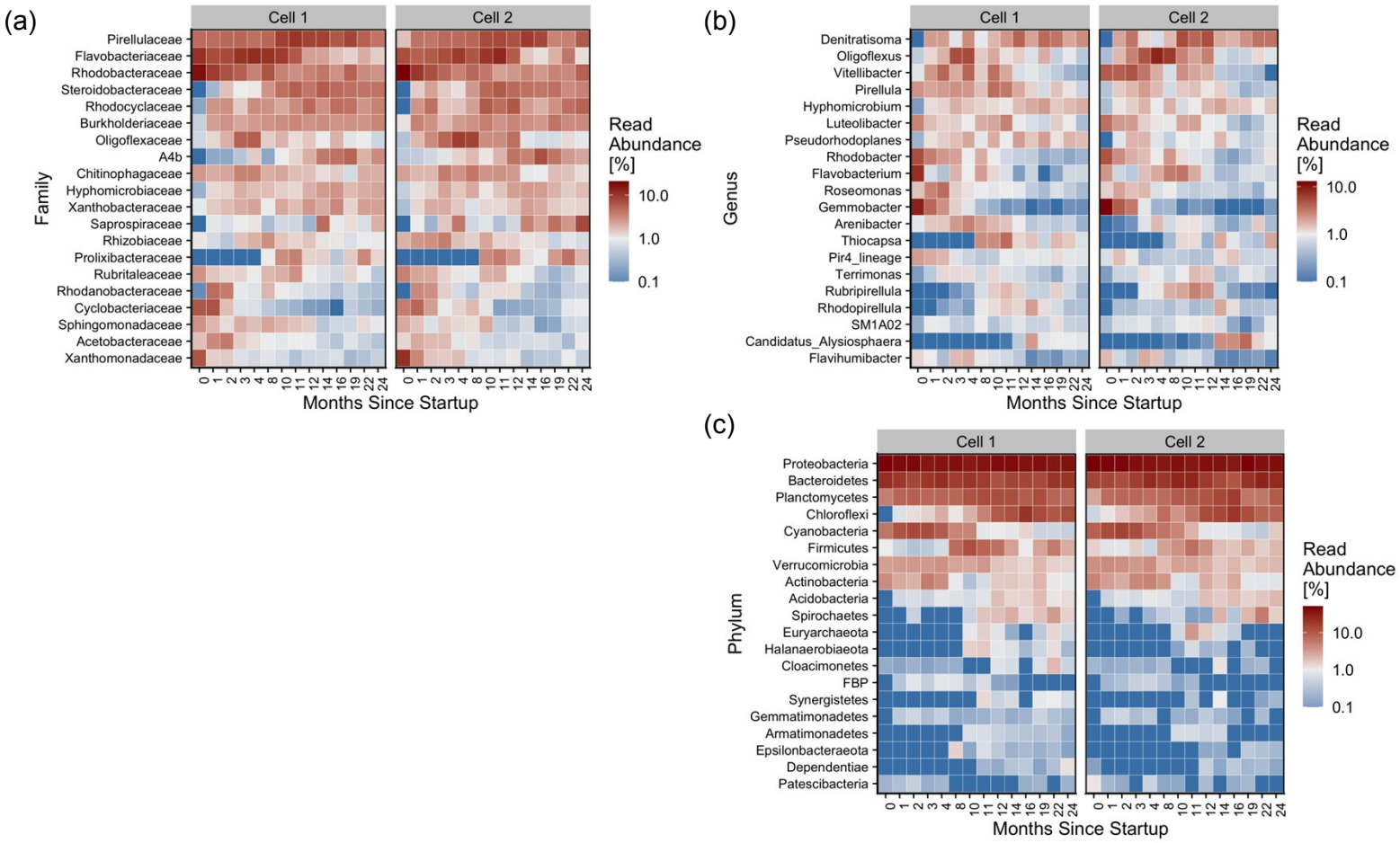

Figure S11. Heatmaps of the top 20 most abundant bacterial and archaeal taxa present in the biomat of Cell 1 and Cell 2, classified to the **(a)** Family, **(b)** Genus, and **(c)** Phylum level. Presented data are from rarefied ASV tables, however analyses were performed on both rarefied and non-rarefied ASV tables. Results were not significantly different.

Table S3. Adonis and beta dispersion statistics comparing differences in weighted and unweighted Unifrac distance matrices between Cell 1 and Cell 2 at every sampling event based on 16S rRNA gene sequencing. Sufficient biomat was not available for triplicate sampling, and therefore adonis testing, during month 0. Communities were never significantly different and the homogeneity of multivariate dispersion assumption was always satisfied. Both rarefied and non-rarefied ASV tables were used as inputs for UniFrac calculations and under no conditions were cells significantly different; only rarefied outputs are shown.

	ADONIS, Weighted UniFrac		**Beta Dispersion, Weighted UniFrac**	**ADONIS, Unweighted UniFrac**		**Beta Dispersion, Unweighted UniFrac**
Date [Months Since Startup]	**R^2**	**p**	**p**	**R^2**	**p**	**p**
8/22/17 [0]	-	-	-	-	-	-
9/27/17 [1]	0.556	0.1	0.501	0.408	0.1	0.501
10/18/17 [2]	0.579	0.1	0.101	0.445	0.1	0.501
11/13/17 [3]	0.316	0.1	0.201	0.339	0.1	0.301
12/13/17 [4]	0.376	0.1	0.301	0.421	0.1	0.501
4/11/18 [8]	0.558	0.1	0.301	0.503	0.1	0.601
6/5/18 [10]	0.747	0.1	0.101	0.458	0.1	0.701
7/10/18 [11]	0.753	0.1	0.801	0.486	0.1	0.801
8/15/18 [12]	0.692	0.1	0.701	0.447	0.1	0.401
10/3/18 [14]	0.072	0.9	0.601	0.133	1.0	0.401
11/28/18 [16]	0.868	0.1	0.701	0.454	0.1	0.401
3/13/19 [19]	0.824	0.1	0.601	0.557	0.1	0.601
6/5/19 [22]	0.752	0.1	0.401	0.532	0.1	0.701
8/28/19 [24]	0.492	0.2	0.801	0.443	0.1	0.601

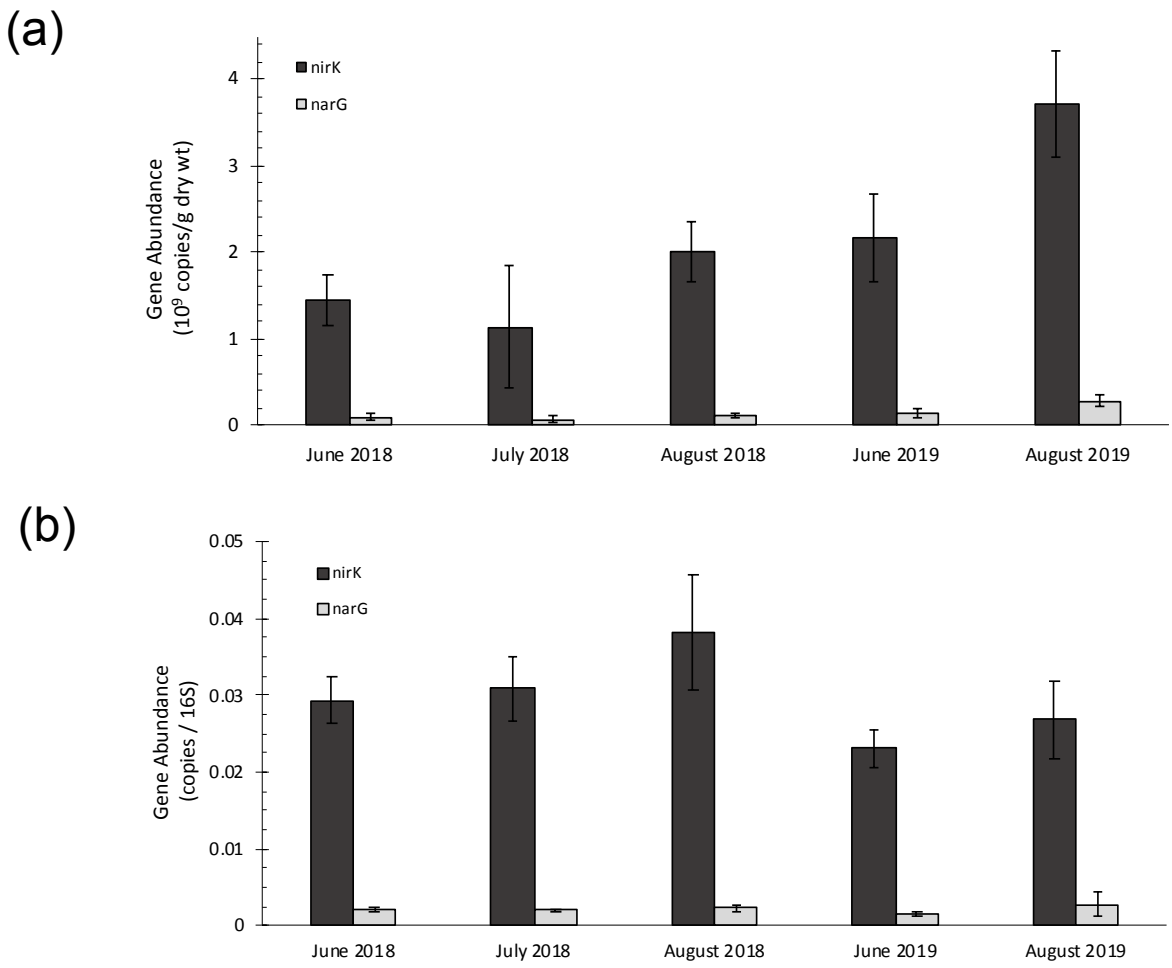

Figure S12. Gene abundance of *nir*K and *nar*G within Cell 1 biomat presented as copies normalized to (a) dry biomat mass, and (b) 16S rRNA gene copies for all inlet samples collected in summer months in 2018 and 2019 (2018: June, July, August; 2019: June, August). Values are presented as average abundances measured in bulk biomat samples collected in triplicate. Only Cell 1 biomat samples were analyzed based on a lack of statistical differences in microbial community composition between Cell 1 and Cell 2 (see Section 2.7 and Table S3).

References

1 A. E. Parada, D. M. Needham and J. A. Fuhrman, Every base matters: Assessing small subunit rRNA primers for marine microbiomes with mock communities, time series and global field samples, *Environ. Microbiol.*, 2016, **18**, 1403–1414.

2 B. W. Stamps, C. N. Lyles, J. M. Suflita, J. R. Masoner, I. M. Cozzarelli, D. W. Kolpin and B. S. Stevenson, Municipal solid waste landfills harbor distinct microbiomes, *Front. Microbiol.*, 2016, **7**, 534.

3 E. A. Kraus, S. R. Beeler, R. A. Mors, J. G. Floyd, GeoBiology 2016, B. W. Stamps, H. S. Nunn, B. S. Stevenson, H. A. Johnson, R. S. Shapiro, S. J. Loyd, J. R. Spear and F. A. Corsetti, Microscale biosignatures and abiotic mineral authigenesis in Little Hot Creek, California, *Front. Microbiol.*, 2018, **9**, 997.

4 B. J. Callahan, P. J. McMurdie, M. J. Rosen, A. W. Han, A. J. A. Johnson and S. P. Holmes, DADA2: High-resolution sample inference from Illumina amplicon data, *Nat. Methods*, 2016, **13**, 581–583.

5 C. Quast, E. Pruesse, P. Yilmaz, J. Gerken, T. Schweer, P. Yarza, J. Peplies and F. O. Glöckner, The SILVA ribosomal RNA gene database project: Improved data processing and web-based tools, *Nucleic Acids Res.*, 2013, **41**, D590–D596.

6 J. G. Caporaso, J. Kuczynski, J. Stombaugh, K. Bittinger, F. D. Bushman, E. K. Costello, N. Fierer, A. G. Peña, J. K. Goodrich, J. I. Gordon, G. A. Huttley, S. T. Kelley, D. Knights, J. E. Koenig, R. E. Ley, C. A. Lozupone, D. Mcdonald, B. D. Muegge, M. Pirrung, J. Reeder, J. R. Sevinsky, P. J. Turnbaugh, W. A. Walters, J. Widmann, T. Yatsunenko, J. Zaneveld and R. Knight, QIIME allows analysis of high- throughput community sequencing data, *Nat. Methods*, 2010, **7**, 335–336.

7 J. G. Caporaso, K. Bittinger, F. D. Bushman, T. Z. Desantis, G. L. Andersen and R. Knight, PyNAST: A flexible tool for aligning sequences to a template alignment, *Bioinformatics*, 2010, **26**, 266–267.

8 M. N. Price, P. S. Dehal and A. P. Arkin, FastTree 2 - Approximately maximum-likelihood trees for large alignments, *PLoS One*, 2010, **5**, e9490.

9 C. Lozupone and R. Knight, UniFrac: A new phylogenetic method for comparing microbial communities, *Appl. Environ. Microbiol.*, 2005, **71**, 8228–8235.

10 P. J. McMurdie and S. Holmes, Phyloseq: An R Package for Reproducible Interactive Analysis and Graphics of Microbiome Census Data, *PLoS One*, 2013, **8**, e61217.

11 J. Podani and I. Miklos, Resemblance Coefficients and the Horseshoe Effect in Principal Coordinates Analysis, *Ecology*, 2002, **83**, 3331–3343.

12 A. J. Oksanen, F. G. Blanchet, M. Friendly, R. Kindt, P. Legendre, D. Mcglinn, P. R. Minchin, R. B. O. Hara, G. L. Simpson, P. Solymos, M. H. H. Stevens and E. Szoecs, Package 'vegan', *R Packag. version 2.0–8*, 2013, 254.

13 M. I. Love, W. Huber and S. Anders, Moderated estimation of fold change and dispersion for RNA-seq data with DESeq2, *Genome Biol.*, 2014, **15**, 1–21.

14 K. S. Andersen, R. H. Kirkegaard, S. M. Karst and M. Albertsen, ampvis2: an R package to analyse and visualise 16S rRNA amplicon data, *bioRxiv*, 2018, 299537.

15 J. C. López-Gutiérrez, S. Henry, S. Hallet, F. Martin-Laurent, G. Catroux and L. Philippot, Quantification of a novel group of nitrate-reducing bacteria in the environment by real-time PCR, *J. Microbiol. Methods*, 2004, **57**, 399–407.

16 S. Henry, E. Baudoin, J. C. López-Gutiérrez, F. Martin-Laurent, A. Brauman and L. Philippot, Quantification of denitrifying bacteria in soils by nirK gene targeted

real-time PCR, *J. Microbiol. Methods*, 2004, **59**, 327–335.
17 J. T. Jasper, Z. L. Jones, J. O. Sharp and D. L. Sedlak, Nitrate removal in shallow, open-water treatment wetlands, *Environ. Sci. Technol.*, 2014, **48**, 11512–11520.
18 S. Turner, K. M. Pryer, V. P. W. Miao and J. D. Palmer, Investigating deep phylogenetic relationships among cyanobacteria and plastids by small subunit rRNA sequence analysis, *J. Eukaryot. Microbiol.*, 1999, **46**, 327–338.
19 R. P. Schwarzenbach, P. M. Gschwend and D. M. Imboden, *Environmental Organic Chemistry*, Wiley, New Jersey, 2nd edn., 2003.
20 W. G. Zumft, Cell biology and molecular basis of denitrification., *Microbiol. Mol. Biol. Rev.*, 1997, **61**, 533–616.
21 M. I. Bellini, D. Kumaresan, S. Tarlera, J. C. Murrell and A. Fernández-Scavino, Identification of active denitrifiers by DNA-stable isotope probing and amplicon sequencing reveals Betaproteobacteria as responsible for attenuation of nitrate contamination in a low impacted aquifer, *FEMS Microbiol. Ecol.*, 2018, **94**, 1–13.
22 H. R. Beller, P. S. G. Chain, T. E. Letain, A. Chakicherla, F. W. Larimer, P. M. Richardson, M. A. Coleman, A. P. Wood and D. P. Kelly, The genome sequence of the obligately chemolithoautotrophic, facultatively anaerobic bacterium Thiobacillus denitrificans, *J. Bacteriol.*, 2006, **188**, 1473–1488.
23 M. Pester, K. H. Knorr, M. W. Friedrich, M. Wagner and A. Loy, Sulfate-reducing microorganisms in wetlands - fameless actors in carbon cycling and climate change, *Front. Microbiol.*, 2012, **3**, 1–19.
24 H. F. Castro, N. H. Williams and A. Ogram, Phylogeny of sulfate-reducing bacteria, 2000, **31**, 1 - 9.
25 S. J. McIlroy and P. H. Nielsen, in *The Prokaryotes: Other Major Lineages of Bacteria and The Archaea*, eds. E. Rosenberg, E. F. DeLong, S. Lory, E. Stackebrandt and F. Thompson, Springer Berlin Heidelberg, Berlin, Heidelberg, 2014, pp. 863–889.
26 E. Ransom-Jones, D. L. Jones, A. J. McCarthy and J. E. McDonald, The Fibrobacteres: An Important Phylum of Cellulose-Degrading Bacteria, *Microb. Ecol.*, 2012, **63**, 267–281.